Glass Stability Changes the Nature of Yielding under Oscillatory Shear

Wei-Ting Yeh,[1] Misaki Ozawa,[2,3] Kunimasa Miyazaki,[1] Takeshi Kawasaki,[1] and Ludovic Berthier[2,4]
[1]Department of Physics, Nagoya University, 464-8602 Nagoya, Japan
[2]Laboratoire Charles Coulomb (L2C), Université de Montpellier, CNRS, 34095 Montpellier, France
[3]Laboratoire de Physique de l'Ecole Normale Supérieure, ENS, Université Paris Sciences et Lettres, CNRS, Sorbonne Université, Université de Paris, F-75005 Paris, France
[4]Department of Chemistry, University of Cambridge, Lensfield Road, Cambridge CB2 1EW, United Kingdom

(Received 28 November 2019; accepted 18 May 2020; published 4 June 2020)

We perform molecular dynamics simulations to investigate the effect of a glass preparation on its yielding transition under oscillatory shear. We use swap Monte Carlo to investigate a broad range of glass stabilities from poorly annealed to highly stable systems. We observe a qualitative change in the nature of yielding, which evolves from ductile to brittle as glass stability increases. Our results disentangle the relative role of mechanical and thermal annealing on the mechanical properties of amorphous solids, which is relevant for various experimental situations from the rheology of soft materials to fatigue failure in metallic glasses.

DOI: 10.1103/PhysRevLett.124.225502

Amorphous solids are generated by decreasing the temperature or by increasing the pressure of supercooled liquids, colloidal suspensions, and granular materials [1–3]. When deformed, their mechanical response is initially elastic but plastic deformations appear at larger strains, which eventually trigger material flow. This elastic-to-plastic transformation is a yielding transition, which is currently an active research topic [4,5]. Understanding the microscopic nature of yielding not only helps in understanding the physics of glasses [6,7], but also guides the design of amorphous materials for industrial applications [8,9].

Yielding in amorphous solids is broadly classified into two classes: ductile and brittle yielding. Ductile materials accumulate plastic activity before yielding and show a smooth crossover from elastic-to-plastic regimes. Many soft glassy materials, such as foams [10], emulsions [11], and colloidal glasses [12], belong to this class. In brittle materials, yielding is characterized by a sharp stress overshoot accompanied by strain localization, which triggers material failure at large deformation. Metallic glasses [9,13], window glasses, and concretes [14] are typical brittle materials.

Brittleness is not necessarily an intrinsic material property. For example, brittleness can gradually increase by changing the cooling rate to prepare the system [15–20] or by physical aging [21–26]. In athermal conditions, this evolution was recently described as a phase transition and confirmed by atomic glass simulations under uniform shear [27]. Evidence was provided that a critical point separates ductile and brittle behaviors, demonstrating the importance of glass stability to understand yielding.

In many studies of the yielding transition, a large amplitude oscillatory shear (LAOS) protocol is used instead of a uniform shear flow. This is useful to relate macroscopic properties with microscopic trajectories of the constituting atoms [28]. LAOS is also the first step toward understanding the response of amorphous solids under dynamical loading conditions [29], relevant to the rheology of soft materials like emulsions and colloids [30,31], and the mechanism of fatigue failure in metallic glasses [32,33]. Previous numerical work under oscillatory shear found that yielding in athermal conditions is associated with a microscopic irreversible transition at the particle level [34–37]. It was also shown that small strain amplitude oscillatory shear can increase glass stability [37–41]. Such "mechanical annealing" [42] was proposed as a route distinct from thermal annealing to prepare stable glasses [43]. When the strain amplitude is increased above yielding, the system cannot find a stable energy state, and the plastic activity associated with energy dissipation is observed at each cycle [34,37,38]. Large-scale simulations [37,39,44] and a mesoscopic model [45,46] in this regime showed that macroscopic shear bands can form at long times, via a mechanism proposed to be similar to shear-band formation under uniform shear at large deformation [47–49]. However, the role of glass preparation on the nature of yielding under oscillatory shear has not been tested over a broad range of glass stabilities. Therefore, the relative role of thermal and mechanical annealings on mechanical properties remains unclear [34,37–40,42–44].

Our goal is to unify the yielding transition of thermally and mechanically annealed systems and to study how yielding changes when glass preparation is varied over a broad enough range to mimic the physics of both colloidal and metallic glasses under oscillatory shear. We use atomistic computer simulations of a simple glass former

over a wide range of preparation temperatures [50]. We carefully disentangle the relative roles of mechanical and thermal annealings and the various physical regimes accessible in the (strain amplitude, preparation temperature) phase diagram, regarding both the nature of the yielding transition and the distinct mechanisms of shear-band formation in different glassy materials.

We simulate a three-dimensional size polydisperse system [50] with a pairwise soft potential given by

$$U(r_{ij}) = \epsilon_0 \left[\left(\frac{d_{ij}}{r_{ij}}\right)^{12} + c_0 + c_1 \left(\frac{r_{ij}}{d_{ij}}\right)^{2} + c_2 \left(\frac{r_{ij}}{d_{ij}}\right)^{4} \right], \quad (1)$$

where $r_{ij} = |\mathbf{r}_i - \mathbf{r}_j|$ is the distance between particles i and j, and $d_{ij} \equiv (d_i + d_j)(1 - 0.2|d_i - d_j|)/2$ controls the nonadditive interaction between particles of diameters d_i and d_j. The cutoff distance of the potential is set to $r_{\rm cut}^{(ij)} = 1.25 d_{ij}$, and the constants c_0, c_1, and c_2 are chosen so that the first and second derivatives of the potential vanish at the cutoff. We, respectively, use the average diameter $\bar{d}$ and energy scale ϵ_0 as our length and energy units. To generate amorphous solids with a broad range of stabilities, we first produce equilibrium configurations of the supercooled liquid over a wide range of temperatures $T_{\rm init}$, using the swap Monte Carlo method [50]. We study the range $T_{\rm init} \in [0.062, 5]$ and work at fixed number density $\rho = 1.02$. These equilibrium configurations are then instantly quenched to zero temperature (using the FIRE algorithm [51]) to form the initial glass configurations to be sheared. The model and physical properties of these glasses were documented in Refs. [27,50,52,53]. In particular, the energy of the inherent structures $E_{\rm IS}$ is almost constant at high $T_{\rm init}$ and starts decreasing as $T_{\rm init}$ drops below the onset temperature $T_{\rm onset} \approx 0.18$. Several physical properties change qualitatively when $T_{\rm init}$ decreases below the mode-coupling crossover temperature $T_{\rm MCT} \approx 0.108$ [53]. The estimated experimental glass temperature is $T_g \approx 0.072$.

We deform these zero-temperature amorphous solids using a simple oscillatory shear with a strain amplitude γ_0 at constant volume. We employ both the athermal quasistatic (AQS) shear protocol [54] and the finite (but small) strain-rate protocol. A homogeneous shear strain is realized using Lees-Edwards boundary conditions [55]. In the AQS protocol, the system is strained at each step by a small incremental strain $|\Delta\gamma| = 2 \times 10^{-4}$, after which the configuration is again relaxed into the nearest energy minimum. In the finite strain-rate protocol, the system is driven by an overdamped dynamical equation [34]

$$\xi \left(\frac{d\mathbf{r}_i}{dt} - \dot{\gamma}(t) \mathbf{r}_i(t) \cdot \hat{\mathbf{y}}\, \hat{\mathbf{x}} \right) + \sum_{j \neq i} \frac{\partial U(r_{ij})}{\partial \mathbf{r}_i} = \mathbf{0}, \quad (2)$$

where $\hat{\mathbf{x}}$ and $\hat{\mathbf{y}}$ are the unit vectors in the x and y directions, $\mathbf{r}_i$ is the position of particle i, and ξ is the friction coefficient that sets the time unit $\bar{d}\xi/\epsilon_0$. The applied strain is $\gamma(t) = \gamma_0 \sin(2\pi t/T_{\rm cyc})$, with an oscillation period $T_{\rm cyc}$. Most reported results are for the finite strain-rate protocol with a small strain-rate $\dot{\gamma}_0 \equiv 2\pi\gamma_0/T_{\rm cyc} = 6.2832 \times 10^{-4}$, and total number of particles $N = 12\,000$. In the Supplemental Material, we show that this finite strain rate is small enough to reproduce results obtained from the AQS limit [56]. Where needed, we also discuss the results of AQS simulations and larger systems $N = 48\,000$. A complete system size dependence is presented in the Supplemental Material [56]. For each data point, we average over at least 50 cycles for at least three different initial conditions after the system reaches a steady state.

Unless specified otherwise, error bars in each figure represent the standard deviation of the measurements.

We first present the behavior of macroscopic rheological quantities in steady state after many cycles. We calculate the linear description of the nonlinear stress-strain relation [28] by fitting the time-dependent shear stress $\sigma(t)$ (see the Supplemental Material [56] for the definition) to $\sigma_0 \sin(2\pi t/T_{\rm cyc} + \delta_0)$, where σ_0 is the stress amplitude and δ_0 is the phase lag. We then obtain the storage modulus as $G' = \sigma_0 \cos(\delta_0)/\gamma_0$. The γ_0 dependence of these quantities is shown in Figs. 1(a)–1(c) for several preparation temperatures $T_{\rm init}$. Data for the less annealed systems, $0.12 \leq T_{\rm init} \leq 5$, whose stabilities would correspond to typical soft materials [27], essentially collapse on curves that are continuous with a cusp at the same yield strain amplitude $\gamma_Y \approx 0.08$ irrespective of $T_{\rm init}$. In Fig. 1(a), σ_0 displays a smooth overshoot at γ_Y, consistent with Refs. [34,37,38]. δ_0 starts to increase sharply in Fig. 1(b),

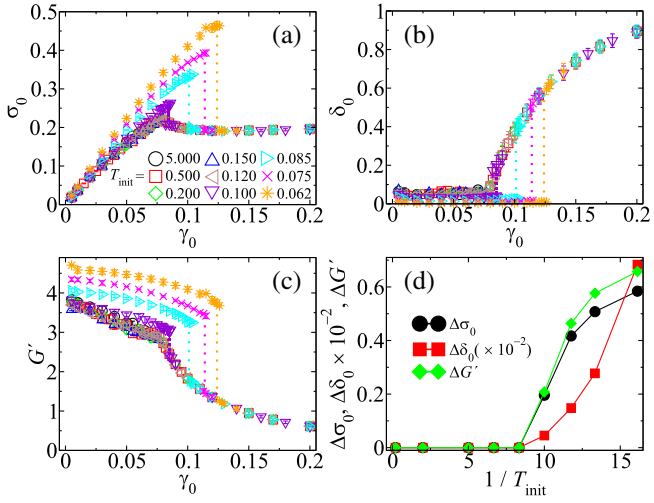

FIG. 1. (a)–(c) Various rheological quantities as a function of the strain amplitude γ_0 for different $T_{\rm init}$'s [see the legend shown in (a)]. (a) Stress amplitude σ_0. (b) Phase lag δ_0. (c) Storage modulus G'. Dashed vertical lines in these figures represent the discontinuous jumps of these quantities. (d) The magnitude of the discontinuities of these quantities at yielding as a function of $1/T_{\rm init}$ vanishes at $T_c \approx 0.1$.

but almost continuously at γ_Y. In Fig. 1(c), G' decreases with a kink at γ_Y, as also shown in Ref. [34]. A qualitatively distinct behavior is observed when $T_{\rm init}$ is below a critical value $T_c \approx 0.1$. The data at small γ_0 no longer collapse and are distinct for each $T_{\rm init}$. One observes that more stable glasses have larger shear and storage moduli and are less dissipative than poorly annealed ones. At the yielding transition point, all data display a sharp discontinuity, which depends on the glass stability. To our knowledge, such large discontinuities were not observed before in computer simulations under oscillatory shear, because it was impossible to produce stable enough glasses [37–41]. Beyond yielding, all curves merge again, as the plastic activity drives the glass away from its stable initial conditions, and memory is eventually lost [37,38]. Interestingly, the number of cycles required to reach the steady state remains finite below T_c in the vicinity of γ_Y, whereas it diverges for poorly annealed systems [34,35,37] (see the Supplemental Material [56]). In Fig. 1(d), we show the magnitude of the jumps of the various rheological quantities at γ_Y as a function of $T_{\rm init}$ (see the Supplemental Material for the precise definitions [56]). This representation eloquently demonstrates that the nature of yielding changes qualitatively at the critical value of $T_c \approx 0.1$. This value is close to the critical temperature discussed in the context of uniform shear [27], but more precise measurements and a finite size scaling analysis would be needed to establish a more precise connection.

To analyze the relative role of thermal and mechanical annealings, we study the dependence of the steady-state inherent structure energy $E_{\rm IS}$ on $T_{\rm init}$ and γ_0, see Fig. 2(a). We again find two qualitatively distinct behaviors, depending on the value of $T_{\rm init}$ before yielding. For $\gamma_0 = 0$, $E_{\rm IS}$ decreases with decreasing $T_{\rm init}$, reflecting the increasing stability of the initial conditions by thermal annealing [53]. For $T_{\rm init} > T_c$, $E_{\rm IS}$ is a decreasing function of γ_0, which confirms that poorly annealed glasses can access deeper energy states when submitted to oscillatory shear of modest amplitude. This is mechanical annealing, as reported in previous works [42,43]. By contrast, for $T_{\rm init} < T_c$ [69], mechanical annealing is not observed. This implies that thermal annealing is so efficient for these glasses that mechanical annealing is no longer able to drive them toward lower energy states. The recent results of Ref. [41] can be interpreted as representative of glasses aged near or slightly below T_c.

Driving poorly annealed glasses above yielding produces instead higher energy configurations, and the yielding transition for those materials appears therefore as a cusp in $E_{\rm IS}$, whereas it again appears as a sharp discontinuity when $T_{\rm init} < T_c$, which emerges at T_c. We conclude that mechanical annealing operates for small γ_0 and high enough $T_{\rm init}$, but becomes inefficient when the effect of thermal annealing increases at low $T_{\rm init}$. The emergence of the critical temperature T_c can be physically understood as a direct consequence of this competition. It corresponds to

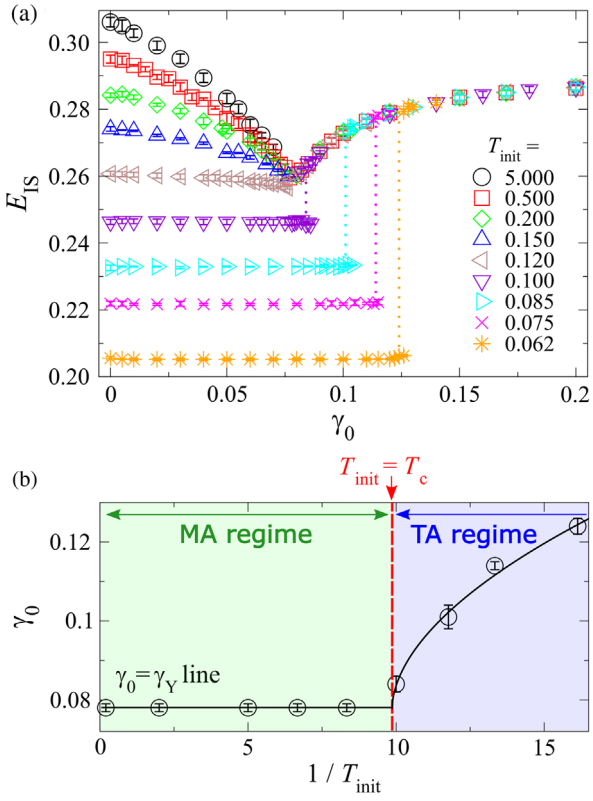

FIG. 2. (a) Steady-state inherent structure energy $E_{\rm IS}$ as a function of the strain amplitude γ_0 for several $T_{\rm init}$. The dashed vertical lines represent the discontinuous jumps. (b) Nonequilibrium phase diagram in the $(\gamma_0, T_{\rm init}^{-1})$ plane. The critical temperature T_c (red long dashed line) divides the phase space into the mechanical annealing (MA) and thermal annealing (TA) regimes. The black solid line separates the elastic and yielded regions (see the text).

the temperature below which mechanical annealing is no longer useful. Since T_c corresponds to a sharp change in the nature of yielding, we see no conceptual reason to relate it to the mode-coupling temperature, which describes a smooth physical crossover in finite dimensions and equilibrium conditions [70]. Physically, lowering T_c decreases the quenched disorder and presumably the density of weak regions in the initial glass configurations [27].

These findings can be summarized in the nonequilibrium phase diagram in the $(\gamma_0, T_{\rm init}^{-1})$ plane shown in Fig. 2(b).

The yield strain amplitude γ_Y separates the "elastic" region at low strain amplitude, where the plastic activity is suppressed in steady state, from the "yielded" region, where plastic events occur during each cycle at large strain amplitude. γ_Y is constant in the regime dominated by mechanical annealing (MA regime) for $T_{\rm init} > T_c$ [38], but it increases with decreasing $T_{\rm init}$ in the regime dominated by thermal annealing (TA regime). The value of T_c can be determined by a power-law fit of γ_Y [56], which gives $T_c \approx 0.101$. Although the nature of yielding changes dramatically with $T_{\rm init}$, it is accompanied for all stabilities

by a similar discontinuous irreversible transition at the particle scale (see, for example, Fig. S9 in the Supplemental Material [56]).

The existence of two distinct regimes for yielding under oscillatory shear also influences the nature of shear banding above yielding. Recent works on the poorly annealed glasses in the AQS limit and small strain rate suggested that persistent shear bands may emerge under slow oscillatory shear for large systems at long times [37,39,44]. We confirm that a persistent shear band forms in our simulations at long times in similar conditions, but it does not appear when the strain rate is large or γ_0 is away from γ_Y [56]. In Fig. 3(a), we illustrate the slow emergence of a shear band after many cycles using AQS simulations and larger system size, $N = 48\,000$, starting from a poorly annealed glass with $T_{\rm init} = 0.5$. In steady shear, the stress-strain rate relation is monotonic and no shear band is formed [71] and thus the observed shear band purely originates from the oscillatory nature of the shearing. A color map of the one-cycle nonaffine deformation $d_{{\rm NA},i}$ for each particle i [72] is used to visualize strain localization after many cycles. To quantify the gradual formation of the shear band, we introduce an order parameter $|H|$, which quantifies the extent of spatial inhomogeneities of $d_{{\rm NA},i}$. See the Supplemental Material for the precise definition of $d_{{\rm NA},i}$ and $|H|$ [56]. In Fig. 3(c), we report the corresponding slow increase of $|H|$. The finite value of $|H|$ at steady state implies the presence of a persistent shear band.

Shear-band formation is very different for $T_{\rm init} < T_c$, as demonstrated in Fig. 3(b). In the first few cycles, a very small amount of localized plastic activity is observed. This is followed by a sudden, macroscopic failure of the material, accompanied by the instantaneous formation of a shear band at $n = 29$ cycles. The shear band is formed within a single cycle, which is very different from the gradual emergence reported for $T_{\rm init} > T_c$ at long times [37,39,44]. The observed behavior is reminiscent of fatigue failure in metallic glasses under cyclic loading in the sense that, after some loading cycles, the system fails abruptly [73]. The time dependence of $|H|$ in Fig. 3(c) confirms the sudden formation of the band, which gradually broadens as the number of cycles increases. At very long times, the memory of the initial condition is lost and both types of systems display similar dynamics.

In this Letter, we systematically analyzed the mechanical properties under oscillatory shear of amorphous solids prepared at different depth in the energy landscape and the interplay between thermal and mechanical annealings. We have identified a critical temperature T_c separating two distinct regimes for yielding. For systems prepared at $T_{\rm init} > T_c$ in the MA regime (corresponding to typical soft materials), mechanical annealing can drive the system toward lower energy states at small strain amplitude, but memory is gradually lost at large strain amplitude. In the TA regime, $T_{\rm init} < T_c$ (corresponding to typical metallic

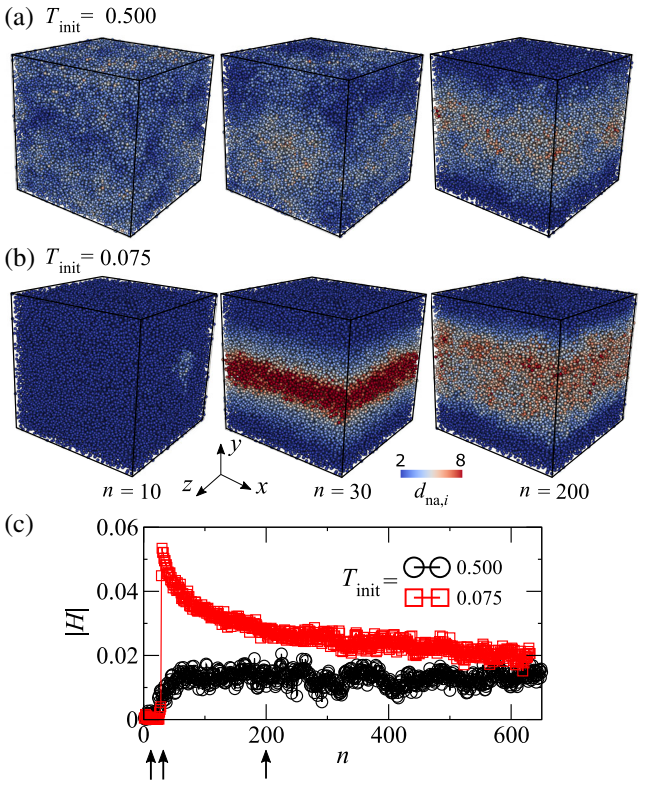

FIG. 3. The snapshots show a color map of the one-cycle nonaffine deformation $d_{{\rm NA},i}$ for (a) $T_{\rm init} = 0.5$ and (b) 0.075 after $n = 10$, 30, and 200 cycles (from top to bottom). (c) Evolution of the shear-band order parameter $|H|$. The arrows indicate the times shown in (a),(b). Yielding in (a) is accompanied by the slow emergence of a diffusive shear band, whereas in (b) a sharp shear band is suddenly formed when the material fails macroscopically. Data obtained using the AQS protocol and $N = 48\,000$ with $\gamma_0 = 0.11$.

glasses), no mechanical annealing occurs at small strain amplitudes, and yielding corresponds to a macroscopic failure of the material accompanied by a discontinuous jump of macroscopic rheological quantities and energy, associated with the sudden appearance of a shear band. Therefore, the MA and TA regimes are separated by a ductile-to-brittle transition. The present Letter dealing with oscillatory shear extends qualitatively similar findings obtained for uniform shear in AQS conditions [27] to time-dependent flows.

We observed distinct mechanisms of shear-band formation in the MA and TA regimes. A shear band forms gradually at long times in the MA regime, becoming persistent in the steady state after yielding. In the TA regime, however, an abrupt emergence of a shear band in a single cycle is found. In particular, before shear-band formation, a small number of localized precursor events are observed [see Fig. 3(b)], which would initiate a macroscopic shear band [74]. Future work should address in more detail the distinct mechanisms for shear banding in

these two regimes. Some preliminary results on this aspect are shown in the Supplemental Material [56].

We investigated the important role of glass stability on the yielding under oscillatory shear relevant for various experimental situations from the rheology of soft materials to fatigue failure in metallic glasses. Our Letter elucidates the interplay between mechanical and thermal annealing processes, providing useful information for material design in industrial applications [75], as well as theoretical descriptions of amorphous materials under cyclic deformation [45,46,76].

We thank Srikanth Sastry for discussions. We also thank the anonymous referee for bringing our attention to Ref. [41]. This research is supported by Japan Society for the Promotion of Science (JSPS) KAKENHI (No. 16H06018, No. 16H04034, No. 18H01188, No. 19K03767, and No. 19H01812) and a grant from the Simons Foundation (No. 454933, L. B.)

[1] P. G. Debenedetti and F. H. Stillinger, Nature (London) **410**, 259 (2001).
[2] C. S. O'Hern, S. A. Langer, A. J. Liu, and S. R. Nagel, Phys. Rev. Lett. **88**, 075507 (2002).
[3] A. J. Liu and S. R. Nagel, Nature (London) **396**, 21 (1998).
[4] D. Bonn, M. M. Denn, L. Berthier, T. Divoux, and S. Manneville, Rev. Mod. Phys. **89**, 035005 (2017).
[5] A. Nicolas, E. E. Ferrero, K. Martens, and J.-L. Barrat, Rev. Mod. Phys. **90**, 045006 (2018).
[6] A. Wisitsorasak and P. G. Wolynes, Proc. Natl. Acad. Sci. U.S.A. **114**, 1287 (2017).
[7] Y. Jin, P. Urbani, F. Zamponi, and H. Yoshino, Sci. Adv. **4**, eaat6387 (2018).
[8] M. Telford, Mater. Today **7**, 36 (2004).
[9] A. L. Greer, Y. Q. Cheng, and E. Ma, Mater. Sci. Eng. R **74**, 71 (2013).
[10] J. Lauridsen, M. Twardos, and M. Dennin, Phys. Rev. Lett. **89**, 098303 (2002).
[11] T. Mason, J. Bibette, and D. Weitz, J. Colloid Interface Sci. **179**, 439 (1996).
[12] P. Schall, D. A. Weitz, and F. Spaepen, Science **318**, 1895 (2007).
[13] T. C. Hufnagel, C. A. Schuh, and M. L. Falk, Acta Mater. **109**, 375 (2016).
[14] J.-I. Sim, K.-H. Yang, E.-T. Lee, and S.-T. Yi, J. Mater. Civ. Eng. **26**, 845 (2014).
[15] M. Utz, P. G. Debenedetti, and F. H. Stillinger, Phys. Rev. Lett. **84**, 1471 (2000).
[16] M. Fan, M. Wang, K. Zhang, Y. Liu, J. Schroers, M. D. Shattuck, and C. S. O'Hern, Phys. Rev. E **95**, 022611 (2017).
[17] J. Shen, Y. Huang, and J. Sun, J. Mater. Res. **22**, 3067 (2007).
[18] J. Ashwin, E. Bouchbinder, and I. Procaccia, Phys. Rev. E **87**, 042310 (2013).
[19] D. Rodney, A. Tanguy, and D. Vandembroucq, Model. Simul. Mater. Sci. Eng. **19**, 083001 (2011).
[20] J. Ketkaew, W. Chen, H. Wang, A. Datye, M. Fan, G. Pereira, U. D. Schwarz, Z. Liu, R. Yamada, W. Dmowski, M. D. Shattuck, C. S. O'Hern, T. Egami, E. Bouchbinder, and J. Schroers, Nat. Commun. **9**, 3271 (2018).
[21] A. L. Volynskii, A. V. Efimov, and N. F. Bakeev, Polym. Sci. Ser. C **49**, 301 (2007).
[22] J. Rottler and M. O. Robbins, Phys. Rev. Lett. **95**, 225504 (2005).
[23] O. A. Hasan, M. C. Boyce, X. S. Li, and S. Berko, J. Polym. Sci., Part B: Polym. Phys. **31**, 185 (1993).
[24] A. Y.-H. Liu and J. Rottler, Soft Matter **6**, 4858 (2010).
[25] F. Varnik, L. Bocquet, and J.-L. Barrat, J. Chem. Phys. **120**, 2788 (2004).
[26] R. L. Moorcroft, M. E. Cates, and S. M. Fielding, Phys. Rev. Lett. **106**, 055502 (2011).
[27] M. Ozawa, L. Berthier, G. Biroli, A. Rosso, and G. Tarjus, Proc. Natl. Acad. Sci. U.S.A. **115**, 6656 (2018).
[28] K. Hyun, M. Wilhelm, C. O. Klein, K. S. Cho, J. G. Nam, K. H. Ahn, S. J. Lee, R. H. Ewoldt, and G. H. McKinley, Prog. Polym. Sci. **36**, 1697 (2011).
[29] P. Forquin, Phil. Trans. R. Soc. A **375**, 20160436 (2017).
[30] E. D. Knowlton, D. J. Pine, and L. Cipelletti, Soft Matter **10**, 6931 (2014).
[31] D. V. Denisov, M. T. Dang, B. Struth, A. Zaccone, G. H. Wegdam, and P. Schall, Sci. Rep. **5**, 14359 (2015).
[32] C.-C. Wang, Y.-W. Mao, Z.-W. Shan, M. Dao, J. Li, J. Sun, E. Ma, and S. Suresh, Proc. Natl. Acad. Sci. U.S.A. **110**, 19725 (2013).
[33] Z. Sha, S. Qu, Z. Liu, T. Wang, and H. Gao, Nano Lett. **15**, 7010 (2015).
[34] T. Kawasaki and L. Berthier, Phys. Rev. E **94**, 022615 (2016).
[35] I. Regev, T. Lookman, and C. Reichhardt, Phys. Rev. E **88**, 062401 (2013).
[36] I. Regev, J. Weber, C. Reichhardt, K. A. Dahmen, and T. Lookman, Nat. Commun. **6**, 8805 (2015).
[37] D. Fiocco, G. Foffi, and S. Sastry, Phys. Rev. E **88**, 020301 (R) (2013).
[38] P. Leishangthem, A. D. S. Parmar, and S. Sastry, Nat. Commun. **8**, 14653 (2017).
[39] A. D. S. Parmar, S. Kumar, and S. Sastry, Phys. Rev. X **9**, 021018 (2019).
[40] P. Das, H. A. Vinutha, and S. Sastry, Proc. Natl. Acad. Sci. U.S.A. **117**, 10203 (2020).
[41] E. Schinasi-Lemberg and I. Regev, Phys. Rev. E **101**, 012603 (2020).
[42] N. V. Priezjev, J. Non-Cryst. Solids **479**, 42 (2018).
[43] P. Das, A. D. S. Parmar, and S. Sastry, arXiv:1805.12476.
[44] N. V. Priezjev, Comput. Mater. Sci. **150**, 162 (2018).
[45] R. Radhakrishnan and S. M. Fielding, Phys. Rev. Lett. **117**, 188001 (2016).
[46] R. Radhakrishnan and S. M. Fielding, J. Rheol. **62**, 559 (2018).
[47] Y. Shi and M. L. Falk, Phys. Rev. Lett. **95**, 095502 (2005).
[48] G. P. Shrivastav, P. Chaudhuri, and J. Horbach, J. Rheol. **60**, 835 (2016).
[49] G. P. Shrivastav, P. Chaudhuri, and J. Horbach, Phys. Rev. E **94**, 042605 (2016).
[50] A. Ninarello, L. Berthier, and D. Coslovich, Phys. Rev. X **7**, 021039 (2017).

[51] E. Bitzek, P. Koskinen, F. Gahler, M. Moseler, and P. Gumbsch, Phys. Rev. Lett. **97**, 170201 (2006).
[52] D. Coslovich, A. Ninarello, and L. Berthier, SciPost Phys. **7**, 077 (2019).
[53] L. Wang, A. Ninarello, P. Guan, L. Berthier, G. Szamel, and E. Flenner, Nat. Commun. **10**, 26 (2019).
[54] C. E. Maloney and A. Lemaître, Phys. Rev. E **74**, 016118 (2006).
[55] A. W. Lees and S. F. Edwards, J. Phys. C **5**, 1921 (1972).
[56] See Supplemental Material at http://link.aps.org/supplemental/10.1103/PhysRevLett.124.225502 for details about measurement protocols, the definition of observed quantities, comparison of the oscillatory and uniform shear protocols, and the relaxation time near the yielding transition, which includes Refs. [57–68].
[57] J. H. Irving and J. G. Kirkwood, J. Chem. Phys. **18**, 817 (1950).
[58] D. Weaire, M. Ashby, J. Logan, and M. Weins, Acta Metall. **19**, 779 (1971).
[59] T. Egami, T. Iwashita, and W. Dmowski, Metals **3**, 77 (2013).
[60] J. Ding, Y. Q. Cheng, and E. Ma, Appl. Phys. Lett. **101**, 121917 (2012).
[61] N. V. Priezjev, Phys. Rev. E **94**, 023004 (2016).
[62] G. Kapteijns, W. Ji, C. Brito, M. Wyart, and E. Lerner, Phys. Rev. E **99**, 012106 (2019).
[63] R. Cabriolu, J. Horbach, P. Chaudhuri, and K. Martens, arXiv:1807.04330.
[64] J. Boschan, D. Vagberg, E. Somfai, and B. P. Tighe, Soft Matter **12**, 5450 (2016).
[65] K. Baumgarten and B. P. Tighe, Soft Matter **13**, 8368 (2017).
[66] V. V. Vasisht, S. K. Dutta, E. Del Gado, and D. L. Blair, Phys. Rev. Lett. **120**, 018001 (2018).
[67] M. O. Lavrentovich, A. J. Liu, and S. R. Nagel, Phys. Rev. E **96**, 020101(R) (2017).
[68] N. C. Keim and P. E. Arratia, Phys. Rev. Lett. **112**, 028302 (2014).
[69] We have not tried to mix thermal and mechanical annealings to access glassy states with lower energies, as done in Ref. [43], since we more easily produce stable glasses using the swap Monte Carlo algorithm [50].
[70] H. Bhaumik, G. Foffi, and S. Sastry (to be published).
[71] M. Singh, M. Ozawa, and L. Berthier, Phys. Rev. Mater. **4**, 025603 (2020).
[72] C. F. Schreck, R. S. Hoy, M. D. Shattuck, and C. S. O'Hern, Phys. Rev. E **88**, 052205 (2013).
[73] Z. Zhang, J. Eckert, and L. Schultz, Metall. Mater. Trans. A **35**, 3489 (2004).
[74] N. V. Priezjev, Metals **10**, 300 (2020).
[75] Y. Sun, A. Concustell, and A. L. Greer, Nat. Rev. Mater. **1**, 16039 (2016).
[76] N. Perchikov and E. Bouchbinder, Phys. Rev. E **89**, 062307 (2014).